Chinese Chemical Letters 35 (2024) 108651

Contents lists available at ScienceDirect

Chinese Chemical Letters

journal homepage: www.elsevier.com/locate/cclet

High-density triple-phase contact points for enhanced photocatalytic CO_2 reduction to methanol

Hanwen Jian[a], Kaiming Deng[a], Tongyu Wang[a], Chengxi Huang[a], Fang Wu[b], Hailing Huo[a], Bo Ouyang[a], Xuan Liu[a], Jingjing Ma[c], Erjun Kan[a,*], Ang Li[a,*]

[a] MIIT Key Laboratory of Semiconductor Microstructure and Quantum Sensing, School of Science, Nanjing University of Science and Technology, Nanjing 210094, China
[b] College of Information Science and Technology, Nanjing Forestry University, Nanjing 210037, China
[c] State Key Laboratory of High-efficiency Utilization of Coal and Green Chemical Engineering, Ningxia University, Yinchuan 750021, China

ARTICLE INFO

Article history:
Received 13 April 2023
Revised 29 May 2023
Accepted 4 June 2023
Available online 8 June 2023

Keywords:
Photocatalysis
CO_2 reduction reaction
Photocatalyst
Triple-phase contact points
Methanol

ABSTRACT

The efficiency of photocatalytic CO_2 reduction reaction (PCRR) is restricted by the low solubility and mobility of CO_2 in water, poor CO_2 adsorption capacity of catalyst, and competition with hydrogen evolution reaction (HER). Recently, hydrophobic modification of the catalyst surface has been proposed as a potential solution to induce the formation of triple-phase contact points (TPCPs) of CO_2 (gas phase), H_2O (liquid phase), and catalysts (solid phase) near the surface of the catalyst, enabling direct delivery of highly concentrated CO_2 molecules to the active reaction sites, resulting in higher CO_2 and lower H^+ surface concentrations. The TPCPs thus act as the ideal reaction points with enhanced PCRR and suppressed HER. However, the initial synthesis of triple-phase photocatalysts tends to possess a lower bulk density of TPCPs due to the simple structure leading to limited active points and CO_2 adsorption sites. Here, based on constructing a hydrophobic hierarchical porous TiO_2 (o-HPT) with interconnected macropores and mesopores structure, we have significantly increased the density of TPCPs in a unit volume of the photocatalyst. Compared with hydrophobic macroporous TiO_2 (o-MacPT) or mesoporous TiO_2 (o-MesPT), the o-HPT with increased TPCP density leads to enhanced photoactivity, enabling a high methanol production rate with 1111.5 μmol g^{-1} h^{-1} from PCRR. These results emphasize the significance of high-density TPCPs design and propose a potential path for developing efficient PCRR systems.

Clean energy and carbon neutrality have become significant worldwide in solving the problem of global warming caused by excessive reliance on fossil fuels [1,2]. Therefore, the photocatalytic CO_2 reduction reaction (PCRR) is increasingly recognized as a crucial method to convert CO_2 into valuable products to recover CO_2 [3–6]. Methanol is an essential product of the PCRR due to its ease of liquefaction for storage and transportation and its potential as an ideal fuel and intermediate chemical feedstock [7–9].

The aqueous solution is an ideal reaction medium for PCRR since water serves as a source of readily available hydrogen and is chemically mild. However, PCRR efficiency in aqueous solution is restricted by the low solubility and mobility of CO_2 in water, poor CO_2 adsorption capacity of catalyst, and the competition of hydrogen evolution reaction (HER) [10,11]. In principle, CO_2 reduction reaction (CRR) is a triple-phase heterogeneous reaction [12]. Researchers identified that a significant factor limiting the efficiency of CRR is the local concentration of CO_2 in the reaction interface [13]. As reported by Sander *et al.*, the ratio of CO_2 molecules to H_2O molecules at 1 atm pressure is approximately 1:1300 [14], indicating that the CO_2 supply during a significant portion of the reaction time is insufficient, particularly when the diffusion rate of CO_2 in aqueous solution is sluggish.

Some researchers have proposed that the hydrophobic surface enables efficient triple-phase contact points (TPCPs) of CO_2 (gas phase), H_2O (liquid phase), and catalyst (solid phase) near the surface of the catalyst, which enables the direct delivery of highly concentrated gas-phase CO_2 molecules to the surface of catalysts. Wang *et al.* revealed that controlling the triphase contact boundary by tuning the wetting state of the electrode is essential for gas-consuming reactions [15]. Li *et al.* broke the mass-transfer limitation of CO_2, inhibited the HER, and enhanced the PCRR by creating a photocatalyst with a hydrophobic surface [11]. Wakerley *et al.* reported that hierarchically structured Cu dendrites with super-

* Corresponding authors.
E-mail addresses: ekan@njust.edu.cn (E. Kan), liang2100@njust.edu.cn (A. Li).

https://doi.org/10.1016/j.cclet.2023.108651
1001-8417/

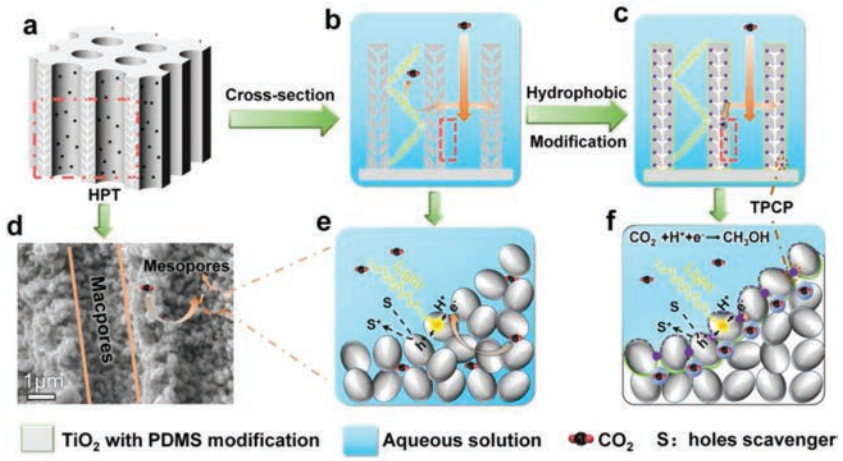

Fig. 1. (a) Schematic of HPT monolithic catalysts. Cross-section structural schematics of (b) HPT and (c) o-HPT. (d) Scanning electron microscope (SEM) image of HPT. Schematics of the local section of (e) HPT and (f) o-HPT. The purple points refer to the triple-phase contact points.

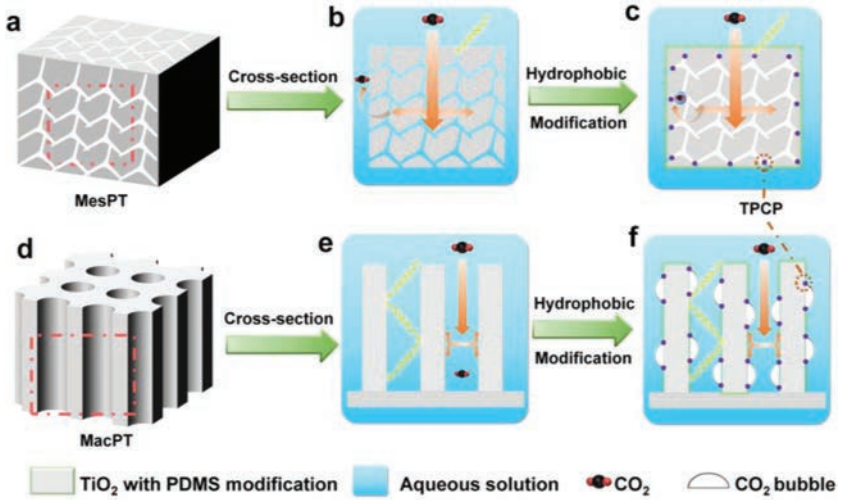

Fig. 2. Schematics of (a) MesPT, (d) MacPT. Cross-section structural schematics of (b) MesPT, (c) o-MesPT, (e) MacPT, (f) o-MacPT. The purple points in (c) and (f) refer to the triple-phase contact points.

hydrophobic surfaces increased the concentration of CO_2 at the interface and consequently increased CO_2 reduction selectivity [12]. With higher CO_2 and lower H^+ surface concentrations, the TPCPs act as ideal reaction points with enhanced PCRR and suppressed HER [16,17]. However, most initial triple-phase photocatalysts can only offer limited TPCPs per unit volume, which may be responsible for the limited catalytic efficiency [18–20].

Here, by constructing a hydrophobic hierarchical porous TiO_2 (o-HPT) with a composite structure of macropores and mesopores, we have significantly increased the density of TPCPs in a unit volume of photocatalyst (Figs. 1a–f), which enables a high methanol production rate with 1111.5 μmol g^{-1} h^{-1} from PCRR. The hierarchical porous TiO_2 (HPT) could provide sufficient active reaction points and enable efficient transport of guest species to framework binding sites [21–24]. We also synthesized mesoporous TiO_2 (MesPT, Figs. 2a–c) or macroporous TiO_2 (MacPT, Figs. 2d–f) as comparative photocatalysts. Hydrophobic modification of MesPT (o-MesPT) or MacPT (o-MacPT) can only increase the TPCP density to a lesser extent due to their single porous structure. The TPCPs can only be formed on the surface of hydrophobic materials [11,12] due to the CO_2 adsorption sites on hydrophilic materials being occupied by water, making it impossible to gather high concentrations of CO_2 [25]. Consequently, TPCPs are only formed at the depth of the surface of the material, which limits the density of TPCPs on o-MesPT (Fig. 2c). And o-MacPT can only generate TPCPs in the form of CO_2 bubbles on the surface (Fig. 2f) [11].

The HPT catalyst was synthesized by spontaneous hydrolysis of titanium isopropoxide (TTIP) in an ammonia solution and then calcinated at 450 °C for 4 h (Section S2 in Supporting information) [26,27]. Most synthesized particles possess macropore channels (Figs. S1a and c in Supporting information). Furthermore, o-HPT was obtained by modifying with PDMS under UV light irradiation (Fig. S2 in Supporting information) [28]. The formation of well-aligned tubular macrochannel arrays is due to the hydrolysis reaction of TTIP with water. This reaction leads to the generation of nanograins that accumulate and form mesopores [29,30]. The resulting macro-mesoporous architecture boasts a high specific surface area (SA) and volume.

The comparative photocatalyst MesPT was synthesized by the hydrolysis of TTIP ethanol solution in distilled water and then applied hydrothermal in the same condition as HPT (Section S3 in Supporting information). MacPT was synthesized by the calcination of the precursor at a higher temperature of 600 °C to collapse its mesoporous structure (Section S4 in Supporting information). With a further increase in temperature above 700 °C, the macropores will also begin to collapse due to crystal phase changes (Fig. S3 in Supporting information) [24]. The hydrophobic modification was also then conducted in MesPT and MacPT.

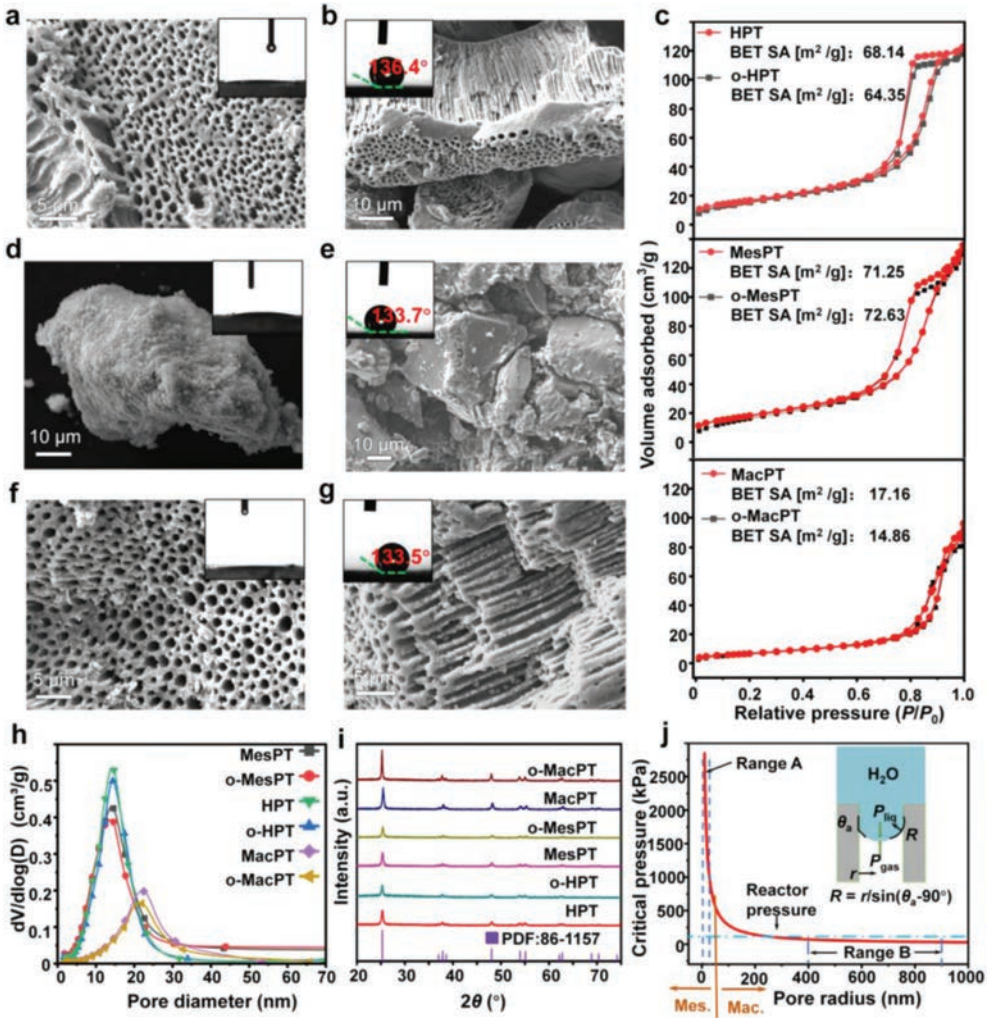

Fig. 3. SEM images and water contact angles (inset) of (a) HPT, (b) o-HPT, (d) MesPT, (e) o-MesPT, (f) MacPT, (g) MacPT. (c) N_2 adsorption and desorption isotherms of HPT and o-HPT, MesPT and o-MesPT, MacPT, and o-MacPT. (h) pore size distribution curves and (i) X-rays diffraction (XRD) patterns of all six catalysts. The unmodified HPT, MesPT, and MacPT are all hydrophilic, in contrast, o-HPT, o-MesPT, and o-MacPT all exhibit excellent hydrophobicity. XRD patterns show that all the catalysts are anatase crystal structures. (j) Critical burst-through pressure of water for the o-HPT as a function of its pore radius *r*. Range A is the size distribution range of mesopores, and Range B is the size distribution range of macropores. Mes. and Mac. are the shorts for mesopore and macropore, respectively. Inset: schematic of the liquid–gas interface inside the pore with a contact angle θ_a greater than 90°.

Scanning electron microscope (SEM) images in Figs. 3a and b show that HPT and o-HPT possess homogenous wormhole-like ordered macrochannel arrays with typical macropore diameters ranging from 0.6 μm to 1.8 μm (Fig. S4a in Supporting information). The macropores dramatically expand the scope for HPT to build complex catalytic reaction environments. Moreover, the N_2 adsorption and desorption isotherms in Fig. 3c show that HPT and o-HPT exhibit type IV isotherms with hysteresis loops at $0.60 < P/P_0 < 1$. This indicates the existence of mesopores and which are produced by the agglomeration of nanoparticles [31,32]. This could be proved in cross-sectional transmission electron microscopy (TEM) images (Figs. S5a and b in Supporting information). The result can be further confirmed by corresponding pore-size distribution curves of HPT and o-HPT in Fig. 3h. Both HPT and o-HPT possess mesopores of relatively uniform size, mainly from 10 nm to 20 nm and average pore size around 11 nm (Table S1 in Supporting information). These results indicate that we have succeeded in synthesizing macro-mesoporous interconnected structure catalysts. The unique three-dimensional tubular structures are expected to significantly decrease the transport resistance of reactants passing through the macrochannel wall and introduce light inside the catalyst bulk, thereby enhancing the reaction rate [33–35].

MesPT exhibits smaller particles of TiO_2 in contrast to HPT (Figs. 3d and e). The TEM image (Fig. S5c in Supporting information) displays the absence of macropores within MesPT, and it is composed of interconnected small TiO_2 particles similar to HPT (Fig. S5d in Supporting information). The N_2 adsorption-desorption isotherms of MesPT and o-MesPT in Fig. 3c show comparable type IV isotherms with HPT and o-HPT, which means that MesPT and HPT have a similar mesoporous structure and pore size (Table S1).

Additionally, the SEM and TEM images of MacPT show a high density of macrochannel arrays throughout the catalysts (Figs. 3f and g, Fig. S5e in Supporting information). The average macropores size of MacPT is 1.37 μm (Fig. S4b in Supporting information). The N_2 adsorption-desorption isotherm of MacPT and o-MacPT shows low adsorption at low relative pressure, which indicates the lack of mesopores [24,31]. However, there is a small hysteresis at higher relative pressure, which means MacPT and o-MacPT possess a small proportion of larger-size mesopores, consistent with pore size distribution curves and the dramatic decrease in both pore volume and BET specific areas (Table S1). According to the previous studies by Yu *et al.*, further heating at 600 °C caused a more severe collapse of the mesoporous framework, resulting in MacPT possessing much fewer mesopores than HPT and

MesPT [21,24]. The mercury intrusion porosimetry (MIP) measurements of HPT and MacPT show that the injection of mercury into the materials mainly occurred at low pressure, suggesting the existence of macropores in these materials. The amount of mercury injected into the MesPT did not increase rapidly at low pressure, indicating no macropores within the MesPT (Fig. S6 in Supporting information).

Fig. 3i shows the X-ray diffraction (XRD) patterns, all corresponding to anatase TiO_2 (JCPDS No. 86–1157), and hydrophobic modification has little effect on the crystal structure. The high-resolution transmission electron microscopy (HRTEM) images of HPT and o-HPT show a lattice spacing of (101) plane of the anatase crystal structure of TiO_2. o-HPT shows a PDMS layer with only a thickness of 1.1 nm (Figs. S7a and b in Supporting information). The thickness of the PDMS layer has a significant influence on photocatalytic performance [36]. The X-ray photoelectron spectroscopy (XPS) full spectrum of o-HPT shows two new peaks corresponding to silicon (Si 2s, Si 2p), indicating the presence of silicon-containing PDMS graft on HPT (Fig. S8 in Supporting information). Moreover, only the outermost surface is hydrophobic; the inside of the mesopore remains intact (Fig. S9 in Supporting information).

The hydrophobicity of catalysts was measured utilizing contact-angle measurement. The results indicate that after hydrophobic modification, all the resulting materials demonstrate excellent hydrophobicity (the inset of Figs. 3b, e, g, and Fig. S10 in Supporting information). To verify that TPCPs can be formed in mesopores, Li *et al*. calculated the anti-flooding capability of the pores (Fig. S11 and Section S8 in Supporting information), which illustrates the robustness of pores in maintaining the triple-phase contact in an aqueous solution [13]. The theoretical model was proposed according to the Young-Laplace equation (Eq. 1, the inset of Fig. 3j),

$$\Delta P = P_{liq} - P_{gas} = 2\sigma/R = 2\sin\left(\theta_a - 90^\circ\right)/r \quad (1)$$

where σ is the surface tension of the liquid, R is the mean radius of curvature of the interface, θ_a is the contact angle, and r is the pore channel radius. For the macropores of o-HPT with a mean pore size of 1.13 μm, the critical burst through pressure during this range is all below the pressure of the reactor with ~80 kPa (Fig. 3j). However, for mesopores with pore sizes in the nanometre scale, the critical burst through pressure up to $\sim 10^3$ kPa (Fig. 3j), which means it is tough for water to enter deep inside the mesopores [37,38]. Therefore o-HPT combines the two kinds of pore structures resulting in a higher density of TPCPs than the other two comparative photocatalysts.

We conducted CO_2 adsorption tests under reactive situations (Fig. S13 and Section S9 in Supporting information) to investigate the effect of hydrophobic treatment of HPT on CO_2 adsorption. The results of the tests showed that the hydrophobic treatment of o-HPT promoted the dissolution rate and the final dissolution amount of CO_2 in water. This finding is consistent with previous studies proposed by other researchers, which suggest that mesoporous material hydrophobization could mitigate the negative effects of water on CO_2 adsorption [39–41].

Other characterizations were performed to further study the impact of PDMS modification on the surface properties of TiO_2. All samples exhibit typical bandgap energy of anatase TiO_2 and remained unaffected after hydrophobic modification (Figs. S14a and b in Supporting information). Additionally, photoluminescence spectra (PL) were used to investigate charge separation efficiency (Fig. S14c in Supporting information), with more vigorous PL intensity indicating the poorer ability of separate charges [42–44]. The results show that PDMS modification did not significantly affect the charge separation efficiency. Fourier transform infrared spectrometer (FT-IR) spectroscopy (Fig. S14d in Supporting information)

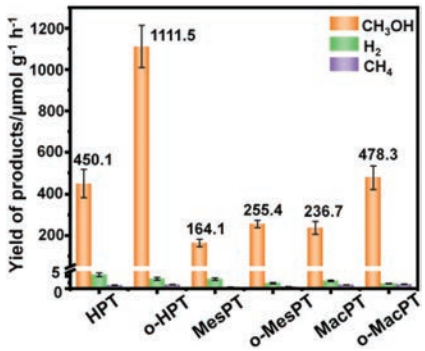

Fig. 4. Photocatalytic CO_2 reduction performance.

test shows that the presence of -CH_3 in the grafted PDMS framework contributed to the hydrophobicity of the o-HPT [28,36,45].

The photoactivity of all the photocatalysts was investigated in $KHCO_3$ (0.1 mol/L) and Na_2SO_3 (0.1 mol/L) aqueous solution under full spectrum irradiation. Na_2SO_3 is a sacrificial reagent for capturing photogenerated holes. Fig. 4 shows that CH_3OH is the primary CO_2 reduction product, along with a small amount of CH_4. In addition, negligible amounts of other carbon derivative products, aside from CH_3OH and CH_4, could be detected (Figs. S15 and S16 in Supporting information). HPT shows the best photocatalytic performance among the hydrophilic catalysts, and the yield of CH_3OH is 450 μmol g^{-1} h^{-1}. This effectively highlights the importance of the hierarchical macro-mesoporous structure for PCRR.

After hydrophobic modification, all three kinds of catalysts showed varying degrees of improvement in the reaction rate. o-HPT had the maximum reaction rate reaching 1111.5 μmol g^{-1} h^{-1}. Pure TiO_2 is limited by its large band gap and low electron transport rate, the performance of PCRR is generally inferior. Most research has focused on loading noble metals and constructing heterogeneous structures to improve performance [46–49]. We have succeeded in making o-HPT perform better than many TiO_2-based catalysts by constructing high-density TPCPs (generally 48.2–454.6 μmol g^{-1} h^{-1}) [17,50–55], which proves the effectiveness of our strategy.

The significantly enhanced photoactivity of o-HPT can be attributed to the increased density of TPCPs. As the schematic we presented based on the above findings in this study (Figs. 1 and 2), HPT exploits the advantage of each porous structure and avoids the disadvantages. Macroporous channels could introduce light inside and transport reactants to the reaction sites [21,35], which addresses the problem of MesPT bulk that cannot be effectively used internally (Figs. 2b and c). The mesopores help to address the lack of sufficient active sites and CO_2 adsorption sites of MacPT to build high-density TPCPs after hydrophobic modification (Figs. 2e and f). Therefore by possessing macrochannels density as high as 5×10^7 cm^{-2} with walls covered with macropores (Section S10 in Supporting information), o-HPT could generate the maximum TPCPs in a unit volume compared to the other two hydrophobic porous structure photocatalysts (o-MesPT and o-MacPT). This results in the highest PCRR methanol production rate. We also performed PCRR tests on hydrophobic P25 (o-P25), which had the lowest performance, demonstrating the importance of porous structure for improving PCRR performance (Fig. S17 in Supporting information).

To clarify the origin carbon source of the CH_3OH and CH_4 formed on o-HPT, three control experiments were conducted (Fig. S18 in Supporting information): (1) CO_2 reduction with H_2O using o-HPT without light; (2) CO_2 reduction with H_2O using light without o-HPT; (3) Reduction of H_2O without CO_2 and $KHCO_3$ over o-HPT with light. The absence of CH_3OH and CH_4 in three control

experiments indicates CH_3OH and CH_4 result from the photocatalytic reduction of CO_2 with H_2O on o-HPT.

In conclusion, we present a promising approach to designing efficient photocatalysts for triple-phase catalytic reactions by emphasizing the importance of high-density TPCPs. We substantially increase TPCP density by constructing hydrophobic hierarchical porous photocatalysts. Compared to catalysts with only mesopores or macropores, o-HPT demonstrates a synergistic effect of macro-mesoporous structure and hydrophobicity. The high density of TPCPs greatly benefits the performance of PCRR as these points serve as effective active sites, resulting in a significantly enhanced methanol production rate. This work presents a promising approach to designing efficient photocatalysts for triple-phase reactions system.

Declaration of competing interest

The authors declare that they have no known competing financial interests or personal relationships that could have appeared to influence the work reported in this paper.

Acknowledgments

We acknowledge the National Natural Science Foundation of China (Nos. 22008121, 11774173, 51790492), the National Outstanding Youth Science Fund Project of National Natural Science Foundation of China (No. T2125004), the Fundamental Research Funds for the Central Universities (Nos. 30920032204, 30920041115), the Foundation of State Key Laboratory of High-efficiency Utilization of Coal and Green Chemical Engineering (No. 2022-K12), Funding of NJUST (No. TSXK2022D002) for financial support.

Supplementary materials

Supplementary material associated with this article can be found, in the online version, at doi:10.1016/j.cclet.2023.108651.

References

[1] R.P. Ye, J. Ding, W.B. Gong, et al., Nat. Commun. 10 (2019) 5698.
[2] A. Li, T. Wang, C.C. Li, et al., Angew. Chem. Int. Ed. 58 (2019) 3804–3808.
[3] A. Li, T. Wang, X.X. Chang, et al., Chem. Sci. 9 (2018) 5334–5340.
[4] Y. Shen, C.J. Ren, L.R. Zheng, et al., Nat. Commun. 14 (2023) 1117.
[5] S.X. Yuan, K. Su, Y.X. Feng, M. Zhang, T.B. Lu, Chin. Chem. Lett. 34 (2023) 107682.
[6] D.F. Gao, W.J. Li, H.Y. Wang, G.X. Wang, R. Cai, Trans. Tianjin Univ. 28 (2022) 245–264.
[7] M. Behrens, F. Studt, I. Kasatkin, et al., Science 336 (2012) 893–897.
[8] P. Zhu, H.T. Wang, Nat. Catal. 4 (2021) 943–951.
[9] T. Amrillah, A.R. Supandi, V. Puspasari, A. Hermawan, Z.W. Seh, Trans. Tianjin Univ. 28 (2022) 307–322.
[10] X.X. Chang, T. Wang, J.L. Gong, Energy Environ. Sci. 9 (2016) 2177–2196.
[11] A. Li, Q. Cao, G.Y. Zhou, et al., Angew. Chem. Int. Ed. 58 (2019) 14549–14555.
[12] D. Wakerley, S. Lamaison, F. Ozanam, et al., Nat. Mater. 18 (2019) 1222–1227.
[13] J. Li, G.X. Chen, Y.Y. Zhu, et al., Nat. Catal. 1 (2018) 592–600.
[14] R. Sander, Atmos. Chem. Phys. Discuss. 14 (2014) 29615–30521.
[15] P.W. Wang, T. Hayashi, Q.A. Meng, et al., Small 13 (2017) 1601250.
[16] S. Wooh, N. Encinas, D. Vollmer, H.J. Butt, Adv. Mater. 29 (2017) 1604637.
[17] X. Liu, C.X. Huang, B. Ouyang, et al., Chem. Eur. J. 28 (2022) e202201034.
[18] R. Kuriki, H. Matsunaga, T. Nakashima, et al., J. Am. Chem. Soc. 138 (2016) 5159–5170.
[19] J.C. Zhang, B. Zhao, W.K. Liang, et al., Adv. Sci. 7 (2020) 2002630.
[20] C.Y. Dong, M.Y. Xing, J.L. Zhang, J. Phys. Chem. Lett. 7 (2016) 2962–2966.
[21] X.C. Wang, J.C. Yu, C.M. Ho, Y.D. Hou, X.Z. Fu, Langmuir 21 (2005) 2552–2559.
[22] T. Wang, X.G. Meng, P. Li, et al., Nano Energy 9 (2014) 50–60.
[23] W. Zhang, Y. Tian, H.L. He, et al., Natl. Sci. Rev. 7 (2020) 1702–1725.
[24] J.G. Yu, Y.R. Su, B. Cheng, Adv. Funct. Mater. 17 (2007) 1984–1990.
[25] J.M. Kolle, M. Fayaz, A. Sayari, Chem. Rev. 121 (2021) 7280–7345.
[26] A. Vantomme, A. Léonard, Z.Y. Yuan, B.L. Su, Colloids Surf. A: Physicochem. Eng. Asp. 300 (2007) 70–78.
[27] X.Y. Wang, H.B. Li, Y. Liu, et al., Appl. Energy 99 (2012) 198–205.
[28] H. Zhou, X. Sheng, Z.Y. Ding, et al., ACS Catal. 12 (2022) 13690–13696.
[29] J.L. Blin, A. Léonard, Z.Y. Yuan, et al., Angew. Chem. Int. Ed. 115 (2003) 2978–2981.
[30] A. Lemaire, J.C. Rooke, L.H. Chen, B.L. Su, Langmuir 27 (2011) 3030–3043.
[31] M. Kruk, M. Jaroniec, Chem. Mater. 13 (2001) 3169–3183.
[32] K. Sing, Pure Appl. Chem. 54 (1982) 2201–2218.
[33] X.C. Li, V.T. John, G.H. He, et al., Langmuir 25 (2009) 7586–7593.
[34] Y. Yuan, J.W. Wang, W.B. Shi, et al., Chin. Chem. Lett. 34 (2023) 107807.
[35] M.A. Isaacs, N. Robinson, B. Barbero, et al., J. Mater. Chem. A 7 (2019) 11814–11825.
[36] J. Liu, L.J. Ye, S. Wooh, et al., ACS Appl. Mater. Interfaces 11 (2019) 27422–27425.
[37] S. Rong, P.C. Su, S.Z. Chen, M.M. Jia, W.B. Li, Chin. Chem. Lett. 33 (2022) 2134–2138.
[38] S.J. Ye, Y.Z. Hou, X. Li, K. Jiao, Q. Du, Trans. Tianjin Univ. 29 (2023) 1–13.
[39] E. Ataeivarjovi, Z.G. Tang, J. Chen, Z.J. Zhao, G. Dong, ACS Sustain. Chem. Eng. 7 (2019) 12125–12137.
[40] M.J. Kang, J.E. Kim, D.W. Kang, et al., J. Mater. Chem. A 7 (2019) 8177–8183.
[41] L.X. Yang, C. Shi, L. Li, Y. Li, Chin. Chem. Lett. 31 (2020) 227–230.
[42] A. Li, X.X. Chang, Z.Q. Huang, et al., Angew. Chem. Int. Ed. 128 (2016) 13938–13942.
[43] A. Li, T. Wang, X.X. Chang, et al., Chem. Sci. 7 (2016) 890–895.
[44] J.Y. Xiong, M.M. Zhang, M.J. Lu, et al., Chin. Chem. Lett. 33 (2022) 1313–1316.
[45] V. Danilov, H.E. Wagner, J. Meichsner, Plasma Process. Polym. 8 (2011) 1059–1067.
[46] K. Kočí, K. Matějů, L. Obalová, et al., Appl. Catal. 96 (2010) 239–244.
[47] S.N. Habisreutinger, L. Schmidt-Mende, J.K. Stolarczyk, Angew. Chem. Int. Ed. 52 (2013) 7372–7408.
[48] Y. Ma, X.L. Wang, Y.S. Jia, et al., Chem. Rev. 114 (2014) 9987–10043.
[49] R.J. Xu, H. Xu, S.B. Ning, et al., Trans. Tianjin Univ. 26 (2020) 470–478.
[50] A. Sharma, B.K. Lee, Catal. Today 298 (2017) 158–167.
[51] X. Cheng, R. Chen, X. Zhu, et al., Energy 120 (2017) 276–282.
[52] X. Li, H.L. Liu, D.L. Luo, et al., Chem. Eng. J. 180 (2012) 151–158.
[53] W.G. Tu, Y.C. Li, L.B. Kuai, et al., Nanoscale 9 (2017) 9065–9070.
[54] W.B. Chen, S.J. Wu, L.Y. Xie, et al., Chem. Eng. J. 464 (2023) 142612.
[55] J.J. Wang, Y.H. Jing, T. Ouyang, Q. Zhang, C.T. Chang, Catal. Commun. 59 (2015) 69–72.